

Pulsation frequency distribution in δ Scuti stars

L.A. Balona¹, J. Daszyńska-Daszkiewicz², A.A. Pamyatnykh³

¹*South African Astronomical Observatory, P.O. Box 9, Observatory, Cape Town, South Africa*

²*Instytut Astronomiczny, Uniwersytet Wrocławski, Kopernika 11, 51-622 Wrocław, Poland*

³*Copernicus Astronomical Center, Bartyleka 18, 00-716 Warsaw, Poland*

Accepted Received ...

ABSTRACT

We study the frequency distributions of δ Scuti stars observed by the *Kepler* satellite in short-cadence mode. To minimize errors in the estimated stellar parameters, we divided the instability strip into ten regions and determined the mean frequency distribution in each region. We confirm that the presence of low frequencies is a property of all δ Scuti stars, rendering meaningless the concept of δ Sct/ γ Dor hybrids. We obtained the true distribution of equatorial rotational velocities in each region and calculated the frequency distributions predicted by pulsation models, taking into account rotational splitting of the frequencies. We confirm that rotation cannot account for the presence of low frequencies. We calculated a large variety of standard pulsation models with different metal and helium abundances, but were unable to obtain unstable low-frequency modes driven by the κ mechanism in any model. We also constructed models with modified opacities in the envelope. Increasing the opacity at a temperature $\log T = 5.06$ by a factor of two does lead to instability of low-degree modes at low frequencies, but also decreases the frequency range of δ Sct-type pulsations to some extent. We also re-affirm the fact that less than half of the stars in the δ Sct instability strip have pulsations detectable by *Kepler*. We also point out the huge variety of frequency patterns in stars with roughly similar parameters, suggesting that nonlinearity is an important factor in δ Sct pulsations.

Key words: stars: oscillations - stars: variables: δ Scuti

1 INTRODUCTION

Delta Scuti stars are main sequence dwarfs and giants with spectral types A0–F5 which pulsate in multiple p, g and mixed modes. They lie on the extension of the Cepheid instability strip towards low luminosities. From ground-based observations, most δ Sct stars are found to pulsate with frequencies in the range $5\text{--}50\text{ d}^{-1}$. The pulsations are driven by the κ mechanism due to partial ionization of He II.

The γ Doradus stars lie in a fairly small region on, or just above, the main sequence that partly overlaps the cool edge of the δ Sct instability strip. They pulsate in multiple g modes with low frequencies (typically less than 5 d^{-1}) and are thought to be driven by a mechanism known as “convective blocking” (Guzik et al. 2000; Dupret et al. 2004). A subset of the δ Sct stars pulsate in both the high and low-frequency ranges and are known as δ Sct/ γ Dor hybrids.

Space photometry from the *Kepler* observatory has completely changed this view. It is found that *all* δ Sct stars pulsate in low-frequency modes, i.e. they are *all* hybrids, (Balona 2014a). The misconception of hybrid δ Sct/ γ Dor stars is due to the fact that low frequencies in δ Sct stars have

sufficiently high amplitudes to be observed from the ground only in a narrow band close to the red edge of the instability strip. The low frequencies in δ Sct stars present a serious problem because standard models predict that low frequencies are stable for δ Sct stars hotter than the granulation boundary. In these hot stars the subsurface convection zone is too thin for convective blocking to drive low-frequency pulsations.

Apart from the problem of low frequencies in hot δ Sct stars, there is the additional problem that the majority of stars in the δ Sct instability strip do not pulsate (Balona & Dziembowski 2011). It is difficult to understand why in two stars with the same physical parameters one star should pulsate as a δ Sct star and the other not pulsate at all, or at least have pulsational amplitudes not detectable in *Kepler* observations. It is possible that nonlinear mode coupling may stabilize the pulsations (Dziembowski 1982; Dziembowski & Krolikowska 1985; Dziembowski et al. 1988) or that the opacity driving mechanism may be saturated (Nowakowski 2005). Since nonlinear models of nonadiabatic nonradial pulsations do not exist, it is not possible, at present, to test these ideas.

Another issue is the fact that A stars appear to be not as simple as previously thought. It has always been supposed that stellar activity ceases for stars hotter than the granulation boundary because the subsurface convection zone is too thin to generate a magnetic field by the dynamo mechanism. Analysis of *Kepler* photometry shows that about 40 per cent of A stars have light variations whose periods closely match the expected rotation periods of these stars, suggesting the presence of starspots (Balona 2011, 2013). Furthermore, about 2 per cent of A stars have flares (Balona 2012, 2013). In fact, the relative number of A-type flare stars is about the same as F and G flare stars and not much smaller than K and M flare stars (Balona 2015). The starspot and flare activity in A stars indicates that we do not fully understand the physics of stellar envelopes which may be related to our lack of understanding of low frequencies in hot δ Sct stars.

Using *Kepler* data, Balona (2014a) showed that low frequencies in δ Sct stars are not stochastically driven, nor can they be explained as nonlinear combinations of high-frequency modes. By comparing the observed distribution of frequencies in *Kepler* δ Sct stars with those from models, Balona (2014a) also showed that the low frequencies cannot be explained as a result of rotational splitting of high-frequency modes.

In order to understand the origin of the low frequencies in δ Sct stars, it is necessary to explore what effects contribute most to the stability or instability of these frequencies in the models. A simple examination of the instability parameter, η , calculated by a nonadiabatic pulsation model will tell us if a particular mode is stable or unstable. However, in order to compare the predicted frequency distribution with observations, it is necessary to simulate rotational splitting of the frequencies as well as other effects. In the absence of mode identification and sufficiently accurate stellar parameters, this is the only way to test if model predictions agree with observations. In order to simulate the effect of rotational splitting, the distribution of true equatorial rotational velocities for the group of stars under study is required. In Balona (2014a) all δ Sct stars were treated as a single group using rotation periods inferred from the light curve.

In this paper we compare the observed and simulated frequency distributions in several regions across the instability strip. Different physical conditions are used for each set of models in an attempt to determine which effects most closely reproduce the observed frequency distributions. In this way we hope to determine whether it is possible to understand the low frequencies under the assumption that they are driven by the κ mechanism. We study mode stability using standard models, i.e. using different abundances and standard opacities, as well as non-standard models, i.e. using opacities which are artificially increased in certain regions in the envelope.

2 THE DATA

The *Kepler* light curves are available as uncorrected simple aperture photometry (SAP) and with pre-search data conditioning (PDC) in which instrumental effects are removed. The vast majority of the stars are observed in long-cadence

(LC) mode with exposure times of about 30 min. Several thousand stars were also observed in short-cadence (SC) mode with exposure times of about 1 min. These data are publicly available on the Barbara A. Mikulski Archive for Space Telescopes (MAST, archive.stsci.edu).

In order to identify δ Sct stars in the *Kepler* field, we calculated the periodograms of over 20 000 stars, including all stars observed in SC mode. By visually examining the light curves and periodograms and using the effective temperatures in the *Kepler* Input Catalogue (KIC, Brown et al. 2011) as a guide, we were able to identify over 1600 δ Sct stars in LC mode and 403 δ Sct stars in SC mode with known stellar parameters. These do not include δ Sct stars in eclipsing binary systems.

The highest pulsation frequency that can be detected in LC mode is about 24 d^{-1} . Since the pulsation frequencies in many δ Sct stars exceed this value, only SC observations allow the unambiguous identification of all pulsation frequencies. Due to variations in heliocentric time correction, the *Kepler* data are not sampled at exactly equal time intervals. In principle, this allows frequencies higher than 24 d^{-1} to be identified in LC data (Murphy et al. 2013). In practice, however, the chance of frequency misidentification is very high for low-amplitude peaks because the difference in peak amplitude between the high- and low-frequency aliases is slight. For this reason, we restrict our analysis to the 403 δ Sct stars observed in SC mode.

To extract all significant frequencies we first calculated the standard Lomb periodogram for unequally-spaced data (Press & Rybicki 1989). The usual technique to extract peaks is that of successive prewhitening. Great caution needs to be exercised in using this method as indiscriminate use leads to a large number of spurious frequencies (Balona 2014b). In effect, only those peaks which are visible in the periodogram of the raw, un-prewhitened data can be considered as significant. Indiscriminate successive prewhitening will extract frequencies which cannot be resolved in the periodogram, even though the extracted amplitudes of such spurious frequencies may be deemed significant. In determining the frequency content of a star, we terminated prewhitening when the peak can no longer be resolved in the original periodogram.

3 SYSTEMATIC AND RANDOM ERRORS

In order to compare the observed frequency distribution with the calculated frequency distribution we need to determine the accuracy of the stellar parameters for individual stars. The stellar parameters derived from Sloan multicolour photometry (without the u band) are listed in the KIC. It is important to determine the systematic and random errors that might be present in the values of effective temperature, T_{eff} , and relative luminosity, $\log L/L_{\odot}$, derived from the KIC parameters.

We do not know the true values of T_{eff} and $\log L/L_{\odot}$ for any δ Sct star, but we can compare the values in the KIC derived from multicolour photometry with the more precise values that can be derived from spectroscopy. Recently, Lehmann et al. (2011); Catanzaro et al. (2010); Niemczura et al. (2015) and Tkachenko et al. (2013) have obtained spectroscopy of several *Kepler* stars from which

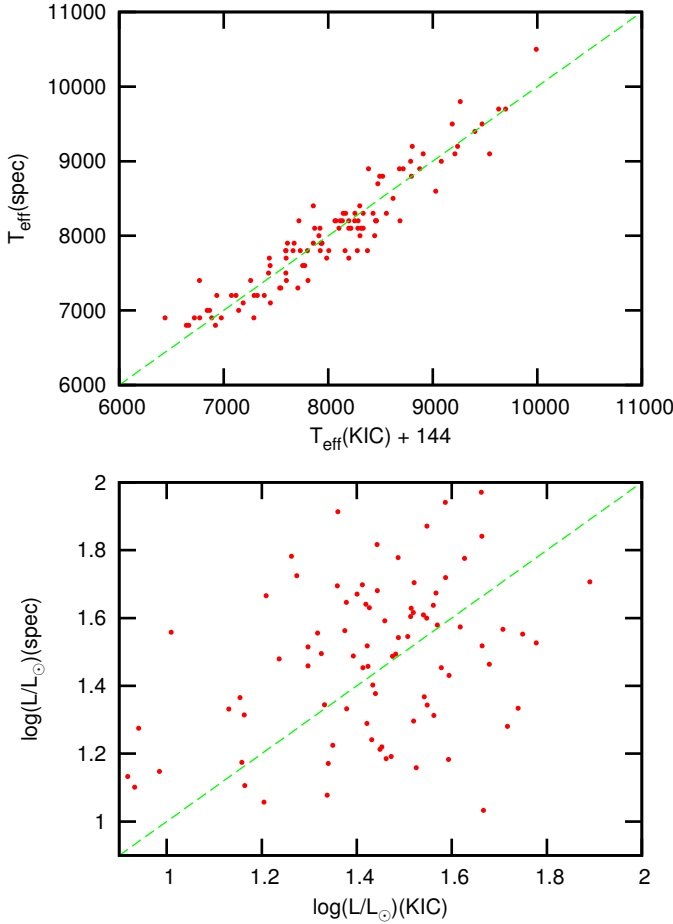


Figure 1. Top panel: the corrected KIC effective temperature as a function of the effective temperature determined by spectroscopic observations of Niemczura et al. (2015). The straight line has unit slope and zero intercept. Bottom panel: the value of $\log(L/L_{\odot})$ derived from the KIC parameters as a function of $\log(L/L_{\odot})$ derived from the spectroscopic parameters. The straight line has unit slope and zero intercept.

stellar parameters are derived. The most numerous observations are those of Niemczura et al. (2015) for which we find a systematic difference in effective temperature $\Delta T_{\text{eff}} = T_{\text{eff}}(\text{spec}) - T_{\text{eff}}(\text{KIC}) = 144 \pm 24$ K from 107 stars with a standard deviation of 253 K per star. There is no significant dependence of ΔT_{eff} on T_{eff} . Since the standard deviation of $T_{\text{eff}}(\text{spec}) \approx 150$ K (Niemczura et al. 2015), we estimate that the standard deviation of $T_{\text{eff}}(\text{KIC}) \approx 200$ K on the assumption that the variances add in quadrature. The top panel of Fig. 1 shows $T_{\text{eff}}(\text{spec})$ from Niemczura et al. (2015) as a function of $T_{\text{eff}}(\text{cor}) = T_{\text{eff}}(\text{KIC}) + 144$.

Given T_{eff} and the surface gravity, $\log g$, the stellar radius may be estimated using the relationship in Torres et al. (2010). This relationship requires the metal abundance which is usually listed among the spectroscopically derived parameters. When the metal abundance is not available, the solar value was used. From the effective temperature and the radius, the relative stellar luminosity, $\log(L/L_{\odot})(\text{spec})$, can be determined. For stars where only KIC values are avail-

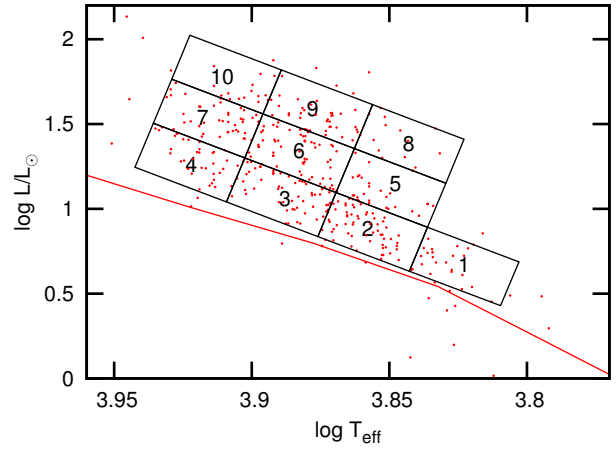


Figure 2. The theoretical H-R diagram showing the SC δ Sct stars (dots) and the designated regions (labeled). The line is the theoretical zero-age main sequence.

able, the luminosity, $\log(L/L_{\odot})(\text{KIC})$ can likewise be estimated from the tabulated effective temperature and radius.

The bottom panel of Fig. 1 shows $\log(L/L_{\odot})(\text{spec})$ as a function of $\log(L/L_{\odot})(\text{KIC})$. The correlation is rather poor, no doubt due to the poor precision of $\log g$ from the photometry. According to Brown et al. (2011) the standard deviation of $\log g$ in the KIC for dwarfs is about 0.4 dex, whereas it is about 0.15 dex from the spectroscopy (Niemczura et al. 2015). As the figure shows, a line of unit slope and zero intercept gives a satisfactory fit. The standard deviation in $\log(L/L_{\odot})$ is 0.26 if the regression is performed with $\log(L/L_{\odot})(\text{KIC})$ as the independent variable or 0.29 as the dependent variable. The standard deviation of $\log(L/L_{\odot})$ derived from the KIC parameters must therefore be about 0.20 dex, since the total variance is the quadratic sum of the two variances.

We used spectroscopically derived parameters whenever possible for each star. When only KIC values are known, we corrected T_{eff} listed by the KIC by 144 K and estimated the luminosity from the KIC radius and uncorrected effective temperature.

Given the large errors in T_{eff} and $\log L/L_{\odot}$, the lack of mode identification, and the profound effect of rotation on the frequency spectrum, it is not possible to model the pulsation frequencies of individual stars. In fact, we are not interested in detailed modeling of a specific star, but only in a comparison of the overall observed and calculated frequency distributions. For this reason we have taken a different approach. We can minimize the uncertainties in effective temperature and luminosity by using the mean values of $\log T_{\text{eff}}$ and $\log L/L_{\odot}$ of many stars in approximately the same location in the instability strip. A good estimate of the mean frequency distribution at this position in the instability strip is obtained by averaging the frequency distributions of these stars. For this purpose we divided the theoretical H-R diagram into ten regions as shown in Fig. 2. These regions were chosen to cover the instability strip as evenly as possible with reasonable resolution while, at the same time,

Table 1. For each region number, N_{Reg} , the number of δ Sct stars, N , in that region and the average number of modes, N_{modes} , having $\nu > 5 \text{ d}^{-1}$ are shown. Also shown is the corresponding range in spectral type, the mean effective temperature, T_{eff} , luminosity, $\log L/L_{\odot}$, surface gravity, $\log g$ and radius, R/R_{\odot} . The last column, $\langle v_e \rangle$ is the mean equatorial rotational velocity (in km s^{-1}) derived from observations of many field stars of the particular spectral type and luminosity class range.

N_{Reg}	N	N_{modes}	Sp.Ty.	$\log T_{\text{eff}}$	$\log L/L_{\odot}$	$\log g$	R/R_{\odot}	$\langle v_e \rangle$
1	29	90	F8V–F3V	3.8253 ± 0.0015	0.6889 ± 0.0152	4.100 ± 0.011	1.654 ± 0.024	40
2	60	252	F4V–A9V	3.8546 ± 0.0012	0.8896 ± 0.0119	4.043 ± 0.009	1.822 ± 0.020	90
3	32	183	F0V–A7V	3.8858 ± 0.0019	1.0922 ± 0.0178	4.003 ± 0.011	1.993 ± 0.030	130
4	25	138	A8V–A4V	3.9146 ± 0.0012	1.2671 ± 0.0190	3.985 ± 0.013	2.136 ± 0.039	150
5	35	238	F5IV–F1IV	3.8537 ± 0.0014	1.0808 ± 0.0136	3.869 ± 0.010	2.280 ± 0.030	70
6	61	245	F1IV–A8IV	3.8837 ± 0.0012	1.3338 ± 0.0130	3.781 ± 0.010	2.663 ± 0.035	110
7	34	220	A8IV–A5IV	3.9121 ± 0.0014	1.4897 ± 0.0148	3.777 ± 0.013	2.793 ± 0.047	140
8	18	103	F5III–F1III	3.8471 ± 0.0022	1.3958 ± 0.0210	3.565 ± 0.016	3.381 ± 0.070	80
9	58	365	F1III–A8III	3.8746 ± 0.0013	1.5508 ± 0.0118	3.551 ± 0.009	3.560 ± 0.041	100
10	15	83	A9III–A6III	3.9043 ± 0.0025	1.7030 ± 0.0181	3.553 ± 0.012	3.692 ± 0.059	110

allowing a fairly large number of stars in each region. The mean effective temperature, luminosity, surface gravity and radius of all δ Sct stars in each region are shown in Table 1.

4 MODE VISIBILITY

In determining the frequency distribution of a particular star we are faced with the problem that individual frequencies are of widely different amplitudes. It would, of course, be preferable to calculate the amplitudes from the models as well. Unfortunately nonlinear calculations of nonradial modes are beyond existing technical capabilities. One approach is to take the linear growth rate as a proxy for the amplitude. However, the final pulsational amplitude attained by a star depends on many factors and not only the initial growth rate. We decided that the most satisfactory method is to ignore amplitude altogether. In other words, a mode of very high amplitude is given the same weight as a mode of very low amplitude. In determining the observed frequency distribution, we simply count the number of significant frequency peaks in the periodogram within a given frequency interval, ignoring their amplitudes.

Using this approach requires that each unstable mode in the models be weighted according to its visibility. It is evident that modes of very high spherical harmonic degree, l , will not be observed because of cancellation effects and cannot therefore be given the same weight as modes of low l . In other words, each unstable mode derived from a model should be assigned a weight equal to its visibility before it can be compared with observations. To calculate the visibility of a mode, we need to discuss the expected relative light amplitude caused by a mode of particular spherical harmonic degree, l , and azimuthal order, m .

The monochromatic light amplitude, $A_{\lambda}(i)$, for a pulsating star whose axis of rotation is inclined at angle i with respect to the observer can be expressed as (Daszyńska-Daszkiewicz et al. 2002):

$$A_{\lambda}(i) = \epsilon Y_l^m(i, 0) b_l^{\lambda} \text{Re}\{D_{1,l}^{\lambda} + D_{2,l} + D_{3,l}^{\lambda}\}.$$

Here ϵ is the intrinsic amplitude, $Y_l^m(i, \phi) = N_{lm} P_l^m(\cos i) e^{im\phi}$ is the spherical harmonic with N_{lm} the normalizing factor and $P_l^m(\cos i)$ the associated Legendre polynomial ($i = \sqrt{-1}$). The disc averaging factor, b_l^{λ}

can be calculated for any particular limb-darkening law. In the above expression, the $D_{1,l}$ term describes the effect of temperature variation on the light amplitude, whereas the influence of effective gravity changes is contained in the $D_{3,l}$ term. The $D_{2,l}$ term describes the effect of variations in projected area on the light amplitude. These terms are given by

$$\begin{aligned} D_{1,l}^{\lambda} &= \frac{1}{4} f \frac{\partial \log \mathcal{F}_{\lambda} |b_l^{\lambda}|}{\partial \log(T_{\text{eff}})}, \\ D_{2,l} &= (2+l)(1-l), \\ D_{3,l}^{\lambda} &= -\left(\frac{3\omega^2}{4\pi\bar{\rho}} + 2\right) \frac{\partial \log \mathcal{F}_{\lambda} |b_l^{\lambda}|}{\partial \log(g_{\text{eff}})}. \end{aligned}$$

The ratio of luminous flux to displacement, f , for each mode is calculated by the nonadiabatic pulsation code. The partial derivatives of the luminous flux, \mathcal{F}_{λ} , with respect to effective temperature, T_{eff} , and with respect to effective gravity, g_{eff} , can be obtained from model atmospheres. The angular pulsation frequency is ω , and $\bar{\rho}$ is the mean density of the star.

If we consider a group of stars in the same region, the visibility of a particular mode for the group is obtained by averaging the various terms in the above equation. Because we are only counting unstable modes, irrespective of amplitude, ϵ is unity if the mode is unstable and zero if it is stable. The average value of $Y_l^m(i, 0)$ is found assuming random orientation of the axis of rotation so that, putting $x = \cos(i)$,

$$\begin{aligned} \langle Y_l^m(i, 0) \rangle &= N_l^m \langle |P_l^m(\cos i)| \rangle, \\ &= N_l^m \frac{2}{\pi} \int_0^1 \frac{|P_l^m(x)|}{\sqrt{1-x^2}} dx, \end{aligned}$$

with

$$N_l^m = \sqrt{\frac{(2l+1)(l-m)!}{4\pi(l+m)!}}.$$

The value of $\langle Y_l^m(i, 0) \rangle$ does not change very much and lies within the range 0.13–0.30 for modes with $l \leq 6$.

The disk-averaging factor, b_l^{λ} , is given by

$$b_l^{\lambda} = \int_0^1 h_{\lambda}(\mu) \mu P_l(\mu) d\mu,$$

where $\mu = \cos \theta$ and θ is the angle in the spherical coordinate system centered on the star. We used the simple limb-darkening law $h(\mu) = 1 + \frac{3}{2}\mu$ independent of wavelength.

Values of b_l drop sharply with l : $b_0 = 1, b_1 = 0.708, \dots b_6 = 0.008$.

In calculating $D_{1,l}$ and $D_{3,l}$ we used the partial derivatives for the Johnson V band computed by Kowalczyk & Daszyńska-Daszkiewicz (2007). The value of $D_{1,l}$ is typically around 40 and $D_{3,l}$ is in the range 2–3. The geometric term, $D_{2,l}$ increases in absolute value with l and is comparable with $D_{1,l}$ for high l . The temperature variation together with b_l dominates the visibility.

5 THE EFFECT OF ROTATION

In a non-rotating star, pulsation modes with the same spherical harmonic degree, l , but with different azimuthal numbers, m , have the same frequency. To first order, the effect of rotation is to remove this degeneracy so that a mode with frequency ν_0 in the non-rotating star appears as $2l + 1$ equally-spaced multiplets with frequencies, ν , given by

$$\nu = \nu_0 + m\nu_{\text{rot}}(1 - C_{nl}),$$

where ν_{rot} is the rotation frequency and C_{nl} is a constant which depends on the structure of the star, l and the radial order, n (Ledoux 1951). The value of C_{nl} is quite small for p modes and hence the frequency splitting may be several cycles per day in the extreme case of high m and large ν_{rot} . The effect of rotation to first order is to introduce a symmetric spread in frequencies.

The above formula breaks down as the rotation rate increases and the splitting is no longer symmetric. The frequency of each multiplet decreases with increasing rotation rate, but the decrease in frequency is greater for larger values of $|m|$. Thus the spread in frequencies is skewed towards low frequencies. It is therefore important to take this effect into account by including higher-order rotational perturbations.

The following formula, (Goupil 2011), is accurate to third order:

$$\omega = \omega_0 - m(1 - C_{nl})\Omega + (D_1 + m^2 D_2)\Omega^2 + m(T_1 + m^2 T_2)\Omega^3,$$

where ω, ω_0 are the perturbed and unperturbed angular pulsation frequencies and Ω is the angular rotation frequency. The values of D_1, D_2, T_1 , and T_2 depend on the mode. In this expression the pulsation and rotation frequencies are in units of the dynamical frequency $\omega_{\text{dyn}} = \sqrt{GM/R^3}$ where G is the gravitational constant, M the stellar mass and R the stellar polar radius. The coefficients have not been calculated for stars in the δ Sct instability strip. However, Reese et al. (2006) lists values for a polytrope of index 3 for $l \leq 3$ and $n \leq 10$.

Since most A stars are moderate or rapid rotators, it is very important to include rotation effects as accurately as possible. Since calculations are only available for polytropes and for limited values of l and n , we are faced with a problem. We decided that the best approach is to use the third-order formula and polytropic values for all p modes. For p modes with $l > 3$ we use the coefficients for $l = 3$. For radial orders greater $n > 10$ we use the values for $n = 10$. This might overestimate the rotational splitting for modes with $l > 3$. Rotational splitting for g modes is smaller than for p modes. We decided to use the first-order formula for all g modes. The distinction between p and g modes is made on the basis of the ratio of the mode kinetic energy in the

gravity-wave propagation zone, E_{kg} , to the total kinetic energy of a mode, E_k , as calculated by the models. We treated modes with $E_{kg}/E_k < 0.5$ as p modes.

To calculate the frequencies of the rotational multiplets in the way just described requires knowledge of the rotation frequency, ν_{rot} . In Balona (2014a) the value of ν_{rot} was obtained from a peak in the periodogram which could be attributed to rotational modulation. We cannot do this because the number of stars with known photometric rotation period is too small (and sometimes zero) in each region. To overcome this problem we have to make the assumption that the distribution of equatorial rotational velocities in a particular region closely corresponds to the distribution of equatorial rotational velocities for field stars with a spectral type and luminosity class appropriate to that region. We used the catalogue of projected rotational velocities compiled by Glebocki & Stawikowski (2000) to determine the distribution of $v \sin i$ for stars in each region. To obtain the distribution of true equatorial rotational velocities, we used the procedure described in Balona (1975). Fig. 3 shows the distribution of $v \sin i$ and the polynomial approximation to the true distribution of equatorial rotational velocities.

6 ASSIGNING WEIGHTS

For a stellar model with a given mass and radius we may calculate the rotational frequency, ν_{rot} , for any given equatorial rotational velocity, v_e . Given ν_{rot} and the calculated frequency of a unstable mode of degree l and radial order n , we may calculate the $2l + 1$ rotationally-perturbed frequencies using the first-order Ledoux formula for g modes and the third-order formula for the p modes. To each of these frequency multiplets we assign the same weight, w_{rot} , which is the probability of finding a star with the particular value of v_e . This weight is calculated using the polynomial fit to the distribution of true equatorial velocities for stars in the appropriate region. We calculated the frequencies and weights of all rotationally-split multiplets using values of v_e from zero to the maximum value in steps of 10 km s^{-1} .

We also assign a weight $w_i = \langle Y_l^m(i, 0) \rangle$ which accounts for the visibility of the mode due to random orientation of the axis of rotation by numerically calculating the integral. This term is relatively unimportant because the w_i does not change much. The visibility due to cancellation effects, $w_b = b_l$, is pre-calculated for any given value of l . Finally we calculate the weight $w_f = D_{1,l} + D_{2,l} + D_{3,l}$ using the values of f, ω and $\bar{\rho}$ from the model as well as the partial derivatives applicable to the given model. The total weight for the mode with frequency ν is $W_\nu = w_{\text{rot}} w_i w_b w_f$. In calculating the predicted frequency distribution we chose a bin size of 1 d^{-1} . The probability at any given frequency, $P(\nu)$, is $P(\nu) = \sum W_\nu$ for all frequencies within this interval.

In principle, the frequency distribution, $P(\nu)$, needs to be calculated for all possible values of l . However, the mode visibility drops sharply with l , so that modes with $l > l_{\text{max}}$ have amplitudes which are so low that they can be ignored. The simplest way to determine l_{max} is to construct frequency distributions using increasing values of l_{max} . We find that there is scarcely any difference in the distributions with $l_{\text{max}} > 4$. We adopted $l_{\text{max}} = 6$ which is certainly adequate for our purposes.

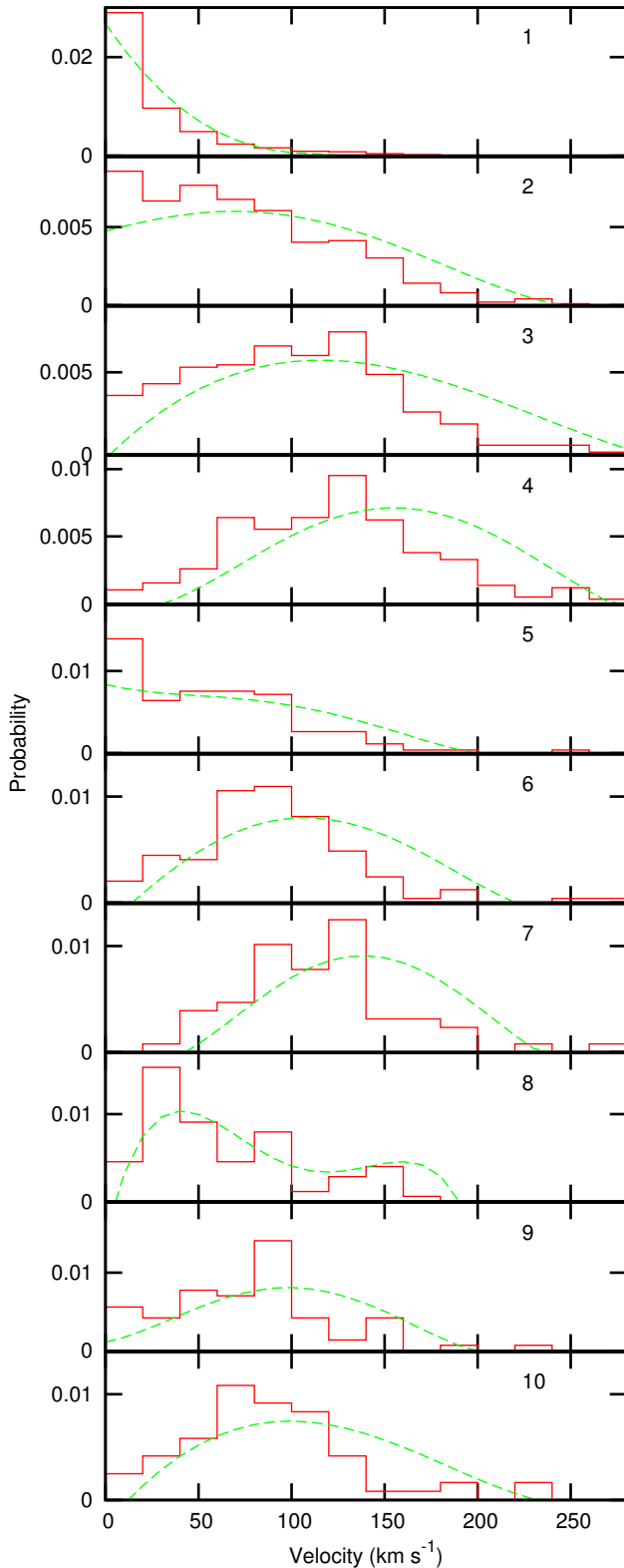


Figure 3. The distribution of projected rotation velocity, $v \sin i$, for field stars with spectral types appropriate for each region is shown by the histogram. The distribution of true equatorial rotational velocities, v_e , is shown by the dashed curve.

In the above procedure we have made assumptions that may not perhaps be entirely justifiable. For example, we assume that all rotationally-split multiplets have the same intrinsic amplitude. We cannot calculate these amplitudes so we do not really know, but this is probably a fair assumption when averaged over many stars. It seems reasonable to assume that stars with approximately the same stellar parameters and rotational velocities have similar frequency distributions. This is certainly the case given our current understanding and that is what the models predict. We shall see below that even this seemingly secure assumption may not be correct.

7 COMPARISON WITH THEORETICAL PREDICTIONS

Equilibrium models were computed using the Warsaw - New Jersey evolution code (Paczynski 1970), assuming two initial hydrogen fractions, $X_0 = 0.70, 0.65$, and four metal abundances, $Z = 0.005, 0.015, 0.030$ and 0.050 . We adopted the chemical element mixture of Asplund et al. (2009) and two sources of the opacity data: OPAL (Rogers & Iglesias 1992) and OP (Seaton 2005). We did not include overshooting from the convective core and used the mixing length parameter $\alpha_{\text{MLT}} = 0.5$ for the convective scale height. We chose this low value of α_{MLT} to eliminate, as far as possible, the fictitious instability of low-frequency modes in the cooler and lower-mass models. This instability is a consequence of the frozen convective flux approximation that we adopted.

We calculated a grid of equilibrium models covering the δ Sct instability strip. The models take rotation into account to first order by applying the centrifugal force correction to local gravity while keeping spherical symmetry. We used a typical initial equatorial rotational velocity of $v_e = 150 \text{ km s}^{-1}$ except for the models with the lowest mass where we used $v_e = 50 \text{ km s}^{-1}$. The effect of rotation is a slight shift of the evolutionary tracks to lower effective temperatures and higher luminosities. The main sequence band is also somewhat extended (see, for example, Breger & Pamyatnykh 1998). Given the fact that we need to determine the rotational frequency splitting over a wide range of rotational velocities corresponding to the known equatorial rotational velocity distribution for a particular group of stars, the value of v_e in the equilibrium model is not an important factor. A non-rotating model would serve our purposes equally well. As explained in the previous section, we used the 3-rd order rotational perturbation only for p modes, while for g modes the 1-st order Ledoux splitting formula was used.

The linear nonadiabatic code of Dziembowski (1977) was used to determine the frequencies and the instability parameter, η , as well as the ratio of luminous flux to displacement, f , for each mode. Only modes with $l \leq 6$ were considered.

In calculating the predicted frequency distribution, we use individual values of $\log T_{\text{eff}}$ and $\log L/L_{\odot}$ for each star in a particular region. The model with temperature and luminosity closest to these values is used to determine the predicted frequency distribution. The average of all frequency distributions for stars in a given region is taken as the best

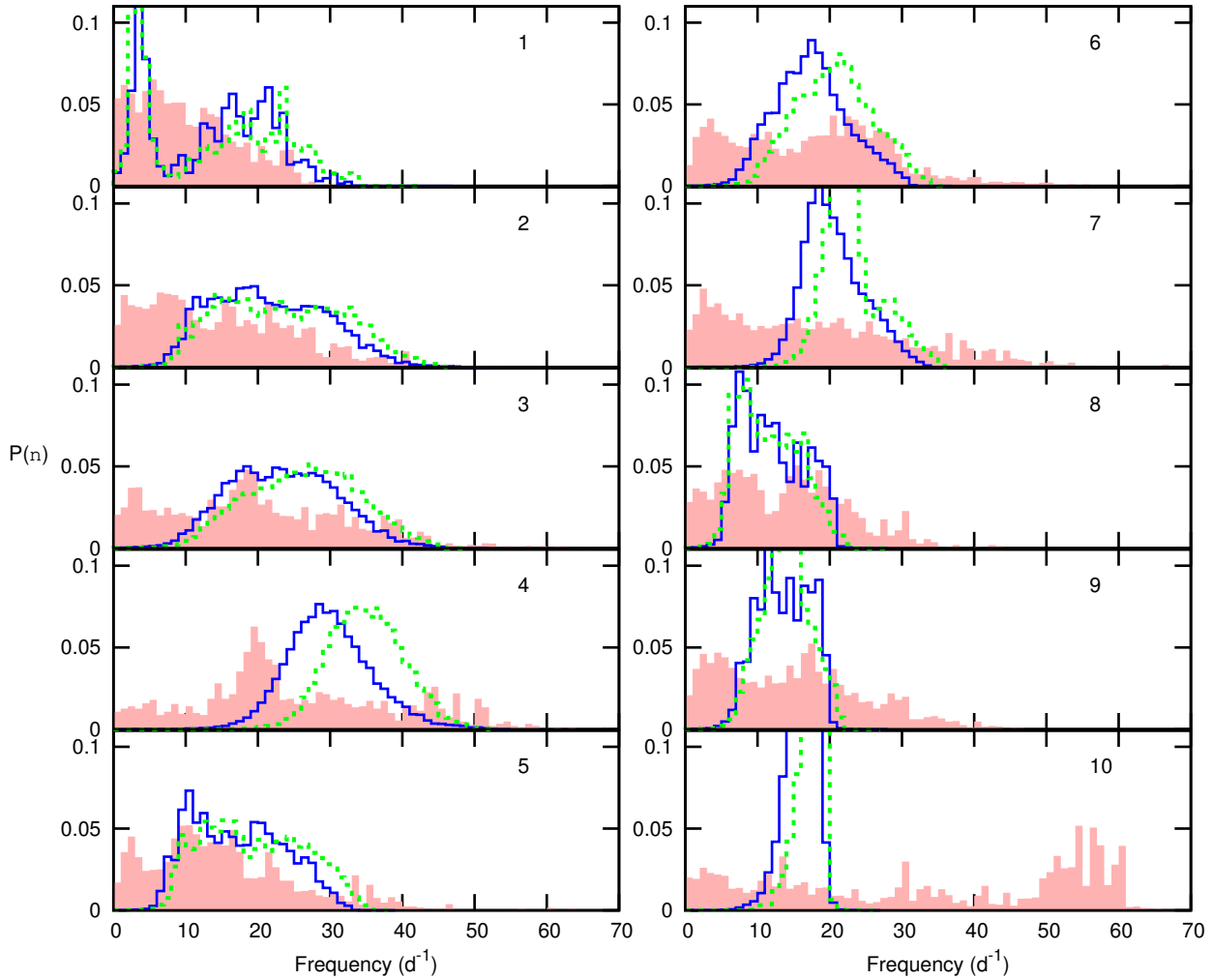


Figure 4. The observed frequency distributions (filled) and the corresponding theoretical frequency distributions derived from pulsation models with metal abundance $Z = 0.015$ (solid blue curves) and $Z = 0.030$ (dotted green curves). Only unstable modes with the degrees, $l \leq 6$ are considered. Each panel shows the frequency distribution corresponding to the labeled region in the H-R diagram of Fig. 2.

approximation of the predicted frequency distribution for that region.

The observed and predicted frequency distributions are shown in Fig. 4 for $Z = 0.015$ and $Z = 0.030$ using OPAL opacities and an initial hydrogen abundance $X_0 = 0.70$. The unstable low frequencies predicted for the models of region 1 are a result of the frozen convection approximation and are fictitious. It can be seen that low frequencies are observed in stars across the whole instability strip. In other words, all δ Sct stars are hybrids. Also, it can be seen that the predicted frequency distributions fail to show frequencies less than about 5 d^{-1} . The same result was obtained with models calculated using OP opacities.

Apart from the disagreement in the low-frequency range, we also note that for the more luminous stars of regions 8, 9 and 10 the observed distributions extend to much higher frequencies than predicted. In general, we expect the observed distribution to be broader than the predicted distribution because each region includes a fraction of stars with true values of T_{eff} and $\log L/L_{\odot}$ which are outside the

region. Even so, it does not seem possible to explain the high-frequency tails of the luminous stars in this way because there is no such tail among the less luminous stars.

What we can definitely conclude from Fig. 4 is that a change in metal abundance cannot explain the mismatch between observations and the models. We also calculated models with $Z = 0.005$ and $Z = 0.050$ which we do not show in Fig. 4 to avoid confusion. The distributions with lower and higher metal abundance are quite similar to those shown in the figure. We also calculated models where the helium abundance is substantially increased so that the initial hydrogen abundance is decreased from $X_0 = 0.70$ to $X_0 = 0.65$, but this does not affect mode stability at all at low frequencies. However, there is a slight increase of the instability parameter, η , at high frequencies. We also studied the effect of modes of higher degree and found a negligible difference in the distributions for modes with $l_{\text{max}} = 6$ and $l_{\text{max}} = 10$.

It could be argued that we have not taken the effect of rotation fully into account and that agreement could be

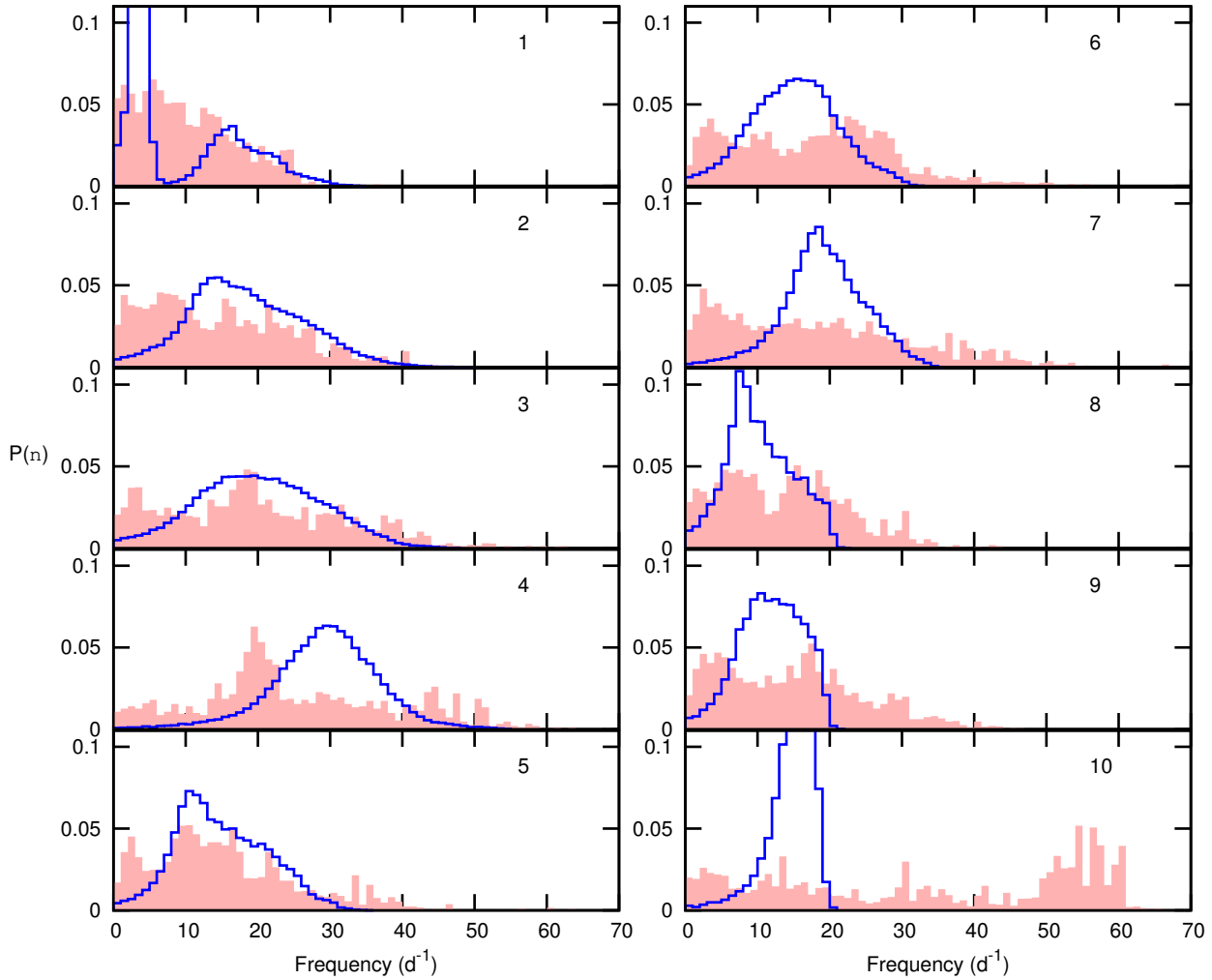


Figure 5. The same as Fig. 4, but we have artificially increased the effect of rotational splitting by using the 3-rd order formula for all modes and setting the disc-averaging factor, b_l , to unity so as to maximize the visibility of modes of high degree where rotational splitting is greatest. Only predicted distributions for $Z = 0.015$ are shown.

achieved by a more realistic treatment of rotational splitting. Unfortunately, we do not have access to non-adiabatic models which take into account stellar distortion, gravity darkening and rapid rotation in a more realistic way. We can, however, take the effect of rotation to extremes by using the 3-rd order perturbation for all modes. We can also enhance the visibility of modes of high degree (which have maximum rotational splitting) by artificially suppressing the disc-averaging factor, b_l (i.e., setting $b_l = 1$ for all modes). The distributions calculated in this way are shown in Fig. 5 for $Z = 0.015$.

Although there is a slight increase in the numbers of low-frequency modes, it is still far too little to match observations. Artificially increasing the effect of rotation in this way also does not assist in explaining the high-frequency tail in luminous stars. We may confidently conclude that there is no possibility that rotational splitting of high-frequency modes can explain the low frequencies.

Since the low frequencies cannot be explained by modi-

fications of standard models, we need to consider other possibilities.

Low frequencies not predicted by models also occur in the β Cep stars. These are early B stars with multiple p, g and mixed modes driven by the opacity bump due to iron group elements (the Z bump). Some low frequencies in these stars can be explained by standard models and some demand increasing the opacity in the Z-bump region (Pamyatnykh et al. 2004). Whether this is the correct solution or how to create the increased opacity is not known. As in the B stars, it is possible that artificially increasing the opacity of δ Sct models in the Z-bump region at $\log T \approx 5.35$ might destabilize the low frequencies.

Recently, Cugier (2012, 2014) found that the OPAL and OP opacities are markedly underestimated in comparison with the Rosseland mean opacities taken from the Castelli & Kurucz (2003) model atmospheres. As a result, a new opacity bump appears at $\log T \approx 5.06$. This bump is due to an attempt to include all spectral lines of atoms in the opacities (Kurucz 2011). This additional opacity bump

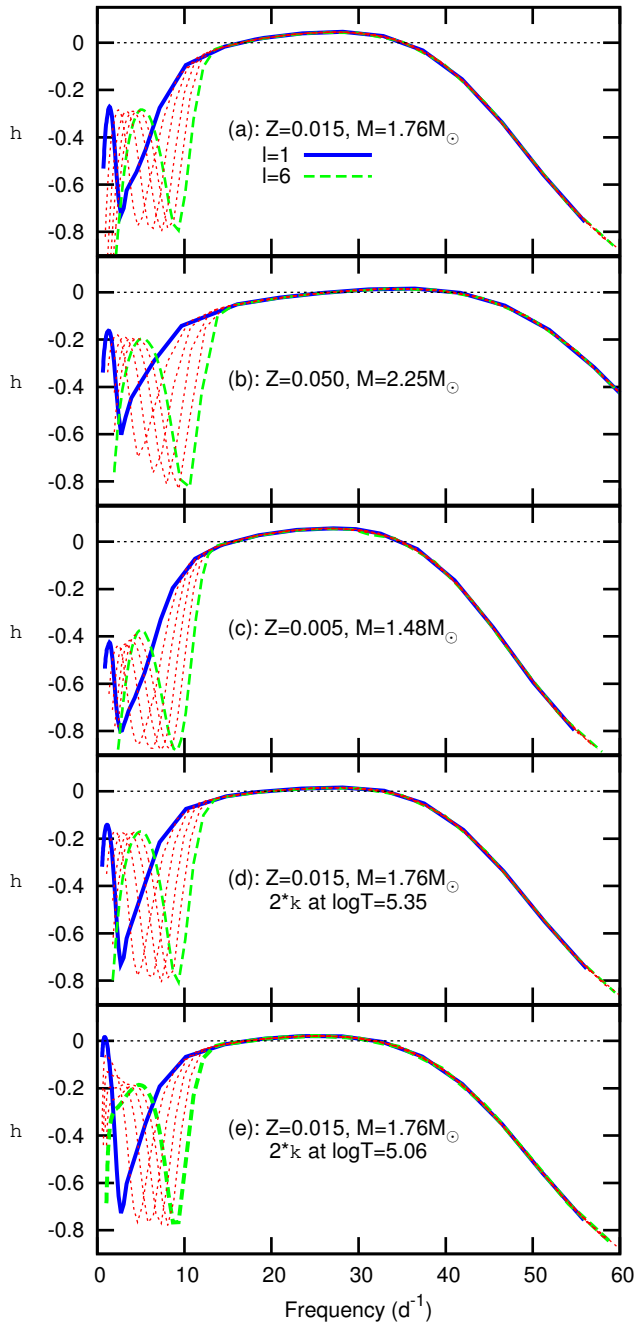


Figure 6. The instability parameter, η , as a function of frequency for modes with $l \leq 6$ for representative models of region 3. All models have $\log T_{\text{eff}} = 3.8855$ and $\log L/L_{\odot} = 1.093$. Panel (a) is a standard model with mass $M = 1.76 M_{\odot}$ and $Z = 0.015$. Panel (b) is a standard model with $M = 2.25 M_{\odot}$ and $Z = 0.050$. Panel (c) is a standard model with $M = 1.48 M_{\odot}$ and $Z = 0.005$. In panel (d) the opacity at $\log T = 5.35$ (the Z-bump region) has been increased by a factor of two. In panel (e) the opacity at $\log T = 5.06$ has been increased by a factor of two to simulate a new opacity bump in the Kurucz opacity data (see main text). All models have initial hydrogen abundance $X_0 = 0.70$.

affects the stability of stellar pulsations and also needs to be considered. In testing the effect of this bump (which we will call the “Kurucz” bump), we did not use the actual Kurucz opacities where the bump occurs, but simulate this additional opacity bump by artificially increasing the standard OPAL opacities in the appropriate temperature range.

In Fig. 6 we show the instability parameter, η , as a function of frequency for $l \leq 6$ in five models with the same effective temperature and luminosity but different metal abundances and enhanced opacities. As one can see, an increase in η in the low frequency range can be obtained either by increasing the value of Z or by an increased opacity in the Z-bump or by increasing the standard OPAL opacities to simulate the Kurucz bump. However, low-frequency modes remain stable except when the Kurucz bump opacity is included. Instability of $l = 1$ modes at low frequencies begins when the standard OPAL opacity in the Kurucz-bump region is increased by a factor of two. Maximum instability occurs when this opacity is increased by a factor of three. Any further opacity increase results in saturation and no further increase in η can occur. Note that an increase in opacity in the Z-bump or Kurucz-bump regions leads to somewhat reduced η for modes with high frequencies. For example, the frequency range of unstable high-frequency modes is decreased from the $15\text{--}35 \text{ d}^{-1}$ range for a standard model to $16\text{--}32 \text{ d}^{-1}$ for a model where the OPAL opacity in the Kurucz bump region is increased by a factor of two.

8 FURTHER UNSOLVED PROBLEMS

Even a cursory inspection of the periodograms of δ Sct stars is sufficient to show the wide variety of frequency patterns in these stars. In fact, each star is unique and can be identified by its periodogram. This is strange because one expects stars with similar effective temperatures, luminosities and rotational velocities to have similar frequency spectra, but this does not seem to be the case. Examples of this effect are shown in Fig. 7 for stars belonging to region 3. The stars shown all have well-determined spectroscopic effective temperatures and surface gravities.

While it is true that the stars may individually have considerably different parameters due to substantial errors in T_{eff} and $\log L/L_{\odot}$, the differences in frequency spectra are very pronounced. This disparity cannot be proved until more accurate parameters are obtained, of course. Nevertheless, it seems that small differences in the parameters may lead to large differences in frequency patterns, implying that nonlinearities in δ Sct envelopes may be very important.

The question of the number of non-pulsating stars in the δ Sct instability strip was addressed by Balona & Dziembowski (2011). They found that most δ Sct stars have effective temperatures in the range $7000 < T_{\text{eff}} < 8500 \text{ K}$ and that even in this range no more than 40–50 per cent of stars pulsate as δ Sct variables. We can confirm this finding. We have found 1165 δ Sct stars in this temperature range in the *Kepler* field observed in long-cadence mode. There are 2839 stars (including the δ Sct stars) in the same temperature range, meaning that only about 41 per cent of stars in the instability strip are detected as δ Sct stars in the *Kepler* photometry.

It could be argued that most of the non- δ Sct stars

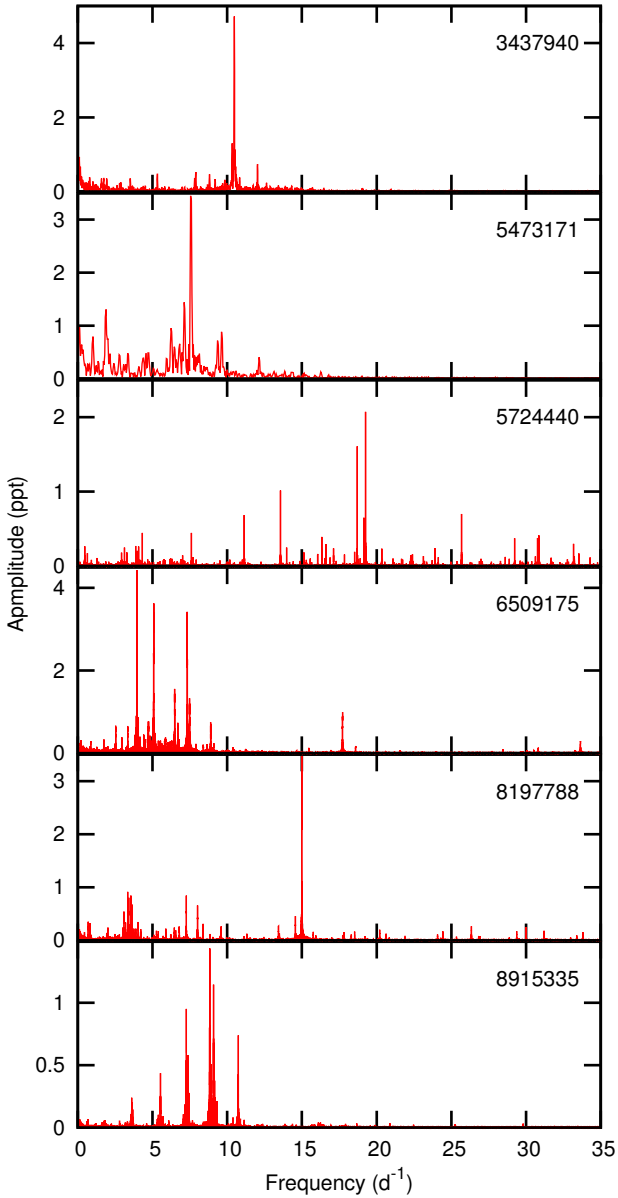


Figure 7. Examples of periodograms of δ Sct stars with similar effective temperatures and luminosities (in region 3). All stars (KIC numbers are shown) have spectroscopic determinations of effective temperature and surface gravity.

are outside the instability strip due to errors in the effective temperature. Errors in luminosity alone play no role because the stars will still be within the instability strip as they can only lie between the ZAMS and TAMS. There are no known high-luminosity stars in this temperature range and in any case none are expected due to the very short lifetimes such stars will have in this evolutionary stage. We have seen that a typical error of about 200 K in T_{eff} can be expected, which is considerably less than the range of 1500 K that we are discussing. The probability that a star in the middle of the instability strip lies, in actual fact, outside the strip is less than 0.01. Of course, the probability will be higher if the star is closer to the edge of the insta-

bility strip, but it means that the probability that all 1674 non-pulsating stars are outside the instability strip is the product of the individual probabilities which is essentially zero. There can be no question that non-pulsating stars are present in the δ Sct instability strip. Of course, it can be argued that the pulsations are less than the detectable limit for *Kepler* (typically less than about 50 ppm). This might be the case, though one can argue against this idea on the basis of the amplitude distribution (Balona & Dziembowski 2011). Such an amplitude disparity, if it exists, still needs an explanation.

9 CONCLUSIONS

We have compared the frequency distributions of groups of δ Sct stars with similar effective temperatures and luminosities with the frequency distributions calculated from pulsation models taking into account, in an approximate but fairly realistic way, the effect of rotational splitting. We have come to the same conclusion as Balona (2014a): that it is impossible to account for frequencies with $\nu < 5 \text{ d}^{-1}$ on the basis that these are high-frequency modes shifted to low frequencies by rotation. Other factors examined in detail in Balona (2014a) are also excluded. The presence of low frequencies is a general feature of all δ Sct stars, no matter where they lie in the instability strip. This is clearly seen in the observed distributions shown in Fig. 4. We also found other inconsistencies between the observed and predicted frequency distributions. For example, the observed distribution for the more luminous stars is much wider than expected. However, this is a minor problem compared to absence of predicted low frequencies.

We calculated a large variety of standard models with differing helium and metal abundances, but in no case could we find unstable modes at low frequencies. The instability parameter, η , does however tend to increase as the metal abundance, Z , increases. We also studied the effect of increasing the opacity at temperatures $\log T = 5.35$ (the Z bump) and the effect of simulating a new opacity bump at $\log T = 5.06$ (the Kurucz bump). The Kurucz bump does not occur in the OPAL and OP opacities, but appears in model atmospheres, as discussed by Cugier (2012, 2014). We found that increasing the opacity in these two regions does increase the value of η . However, low-frequency modes remain stable unless the OPAL opacities at $\log T = 5.06$ are increased by at least a factor of two to simulate the Kurucz bump or if the opacity in the Z bump is increased by a factor of at least three. At the same time, the range of high-frequency modes is decreased to some extent. We do not claim that this opacity increase is the solution to the problem of low frequencies in δ Scuti stars, but only that there is a likely problem with current opacity data and that further investigation into the sources of opacity in this region are required.

A problem of equal importance is the question of why there are so many non-pulsating stars in the δ Sct instability strip. This could simply be that the *Kepler* photometry is not sufficiently precise to detect such pulsations. This does not resolve the problem because it would not explain the very large disparity in amplitudes among the δ Sct stars. We are clearly faced with substantial problems in the physics of A–F stars.

Recently, further problems in our current understanding of stellar pulsations have come to light. It seems that there are a group of pulsating stars with high frequencies lying between the cool end of the β Cep instability strip and the hot end of the δ Sct instability strip. These were recently investigated by Balona et al. (2015) using *Kepler* and K2 data. Standard models cannot reproduce these pulsations, though it is possible that these so-called “Maia” variables may be rapidly-rotating SPB stars. The unexplained presence of low frequencies in a well-studied group such as the δ Sct stars shows that we still do not fully understand the physics and/or envelopes of hot stars. Until we have a better understanding of the low frequencies in A stars we are not likely to make much progress with the more complex problem of explaining the origin of high frequencies in Maia variables.

ACKNOWLEDGMENTS

The authors wish to thank the *Kepler* team for their generosity in allowing the data to be released to the Kepler Asteroseismic Science Consortium (KASC) ahead of public release and for their outstanding efforts which have made these results possible. Funding for the *Kepler* mission is provided by NASA’s Science Mission Directorate.

LAB wishes to thank the National Research Foundation of South Africa for financial support. JDD and AAP acknowledge partial financial support from the Polish NCN grants 2011/01/B/ST9/05448 and 2011/01/M/ST9/05914.

REFERENCES

- Asplund M., Grevesse N., Sauval A. J., Scott P., 2009, *ARA&A*, 47, 481
- Balona L. A., 1975, *MNRAS*, 173, 449
- , 2011, *MNRAS*, 415, 1691
- , 2012, *MNRAS*, 423, 3420
- , 2013, *MNRAS*, 431, 2240
- , 2014a, *MNRAS*, 437, 1476
- , 2014b, *MNRAS*, 439, 3453
- , 2015, *MNRAS*, 447, 2714
- Balona L. A., Baran A. S., Daszynska-Daszkiewicz J., De Cat P., 2015, *MNRAS*, in press
- Balona L. A., Dziembowski W. A., 2011, *MNRAS*, 417, 591
- Breger M., Pamyatnykh A. A., 1998, *A&A*, 332, 958
- Brown T. M., Latham D. W., Everett M. E., Esquerdo G. A., 2011, *AJ*, 142, 112
- Castelli F., Kurucz R. L., 2003, in *IAU Symposium*, Vol. 210, *Modelling of Stellar Atmospheres*, Piskunov N., Weiss W. W., Gray D. F., eds., p. 20P
- Catanzaro G., Frasca A., Molenda-Żakowicz J., Marilli E., 2010, *A&A*, 517, A3
- Cugier H., 2012, *A&A*, 547, A42
- , 2014, *A&A*, 565, A76
- Daszyńska-Daszkiewicz J., Dziembowski W. A., Pamyatnykh A. A., Goupil M., 2002, *A&A*, 392, 151
- Dupret M., Grigahcène A., Garrido R., Gabriel M., Scuflaire R., 2004, *A&A*, 414, L17
- Dziembowski W., 1977, *AcA*, 27, 95
- , 1982, *Acta Astronomica*, 32, 147
- Dziembowski W., Krolikowska M., 1985, *Acta Astronomica*, 35, 5
- Dziembowski W., Krolikowska M., Kosovitch A., 1988, *Acta Astronomica*, 38, 61
- Glebocki R., Stawikowski A., 2000, *AcA*, 50, 509
- Goupil M.-j., 2011, *ArXiv e-prints*
- Guzik J. A., Kaye A. B., Bradley P. A., Cox A. N., Neuforge C., 2000, *ApJ*, 542, L57
- Kowalczyk L., Daszyńska-Daszkiewicz J., 2007, <http://helas.astro.uni.wroc.pl>
- Kurucz R. L., 2011, *Canadian Journal of Physics*, 89, 417
- Ledoux P., 1951, *ApJ*, 114, 373
- Lehmann H., Tkachenko A., Semaan T., Gutiérrez-Soto J., Smalley B., Briquet M., Shulyak D., Tsymbal V., De Cat P., 2011, *A&A*, 526, A124
- Murphy S. J., Shibahashi H., Kurtz D. W., 2013, *MNRAS*, 430, 2986
- Niemczura E., Murphy S. J., Smalley B., Uytterhoeven K., Pigulski A., Lehmann H., Bowman D. M., Catanzaro G., van Aarle E., Bloemen S., Briquet M., De Cat P., Drobek D., Eyer L., Gameiro J. F. S., Gorlova N., Kaminski K., Lampens P., Marcos-Arenal P., Papics P. I., Vandenbussche B., Van Winckel H., Steslicki M., Fagas M., 2015, *ArXiv e-prints*
- Nowakowski R. M., 2005, *AcA*, 55, 1
- Paczyński B., 1970, *AcA*, 20, 47
- Pamyatnykh A. A., Handler G., Dziembowski W. A., 2004, *MNRAS*, 350, 1022
- Press W. H., Rybicki G. B., 1989, *ApJ*, 338, 277
- Reese D., Lignières F., Rieutord M., 2006, *A&A*, 455, 621
- Rogers F. J., Iglesias C. A., 1992, *ApJS*, 79, 507
- Seaton M. J., 2005, *MNRAS*, 362, L1
- Tkachenko A., Lehmann H., Smalley B., Uytterhoeven K., 2013, *MNRAS*, 431, 3685
- Torres G., Andersen J., Giménez A., 2010, *A&A Rev.*, 18, 67